Supplementary Material

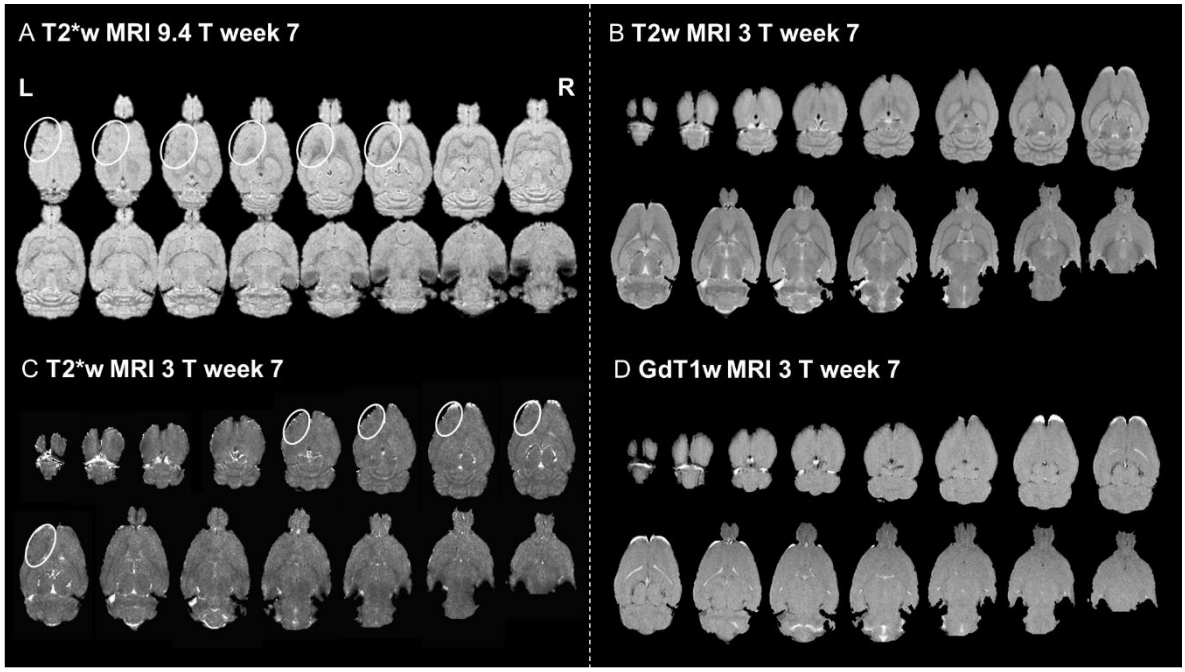

Figure S1. MRI examinations obtained at **(A)** 9.4 T or **(B-D)** 3 T for the Group A rat displayed in **Figure 2A**. (A) T2*w images from rostral to caudal sections performed at week 7 following a single course of pFUS+MB treatment. Hypointense voxels in the anterior left cortex (ellipse) are detected starting from the surface of the brain. Right hippocampal area does not show evidence of pathology. (B) T2w images obtained at week 7 following the pFUS+MB treatment. There was no change on the T2w images compared to images obtained at week 2. (C) T2*w images at 3 T from rostral to caudal sections performed at week 7 following a single pFUS+MB treatment. Hypointense voxels in the anterior left cortex (ellipse) are detected starting from the top of the brain. (D) Post GdT1w images show no evidence of BBB opening. L=left, R=right.

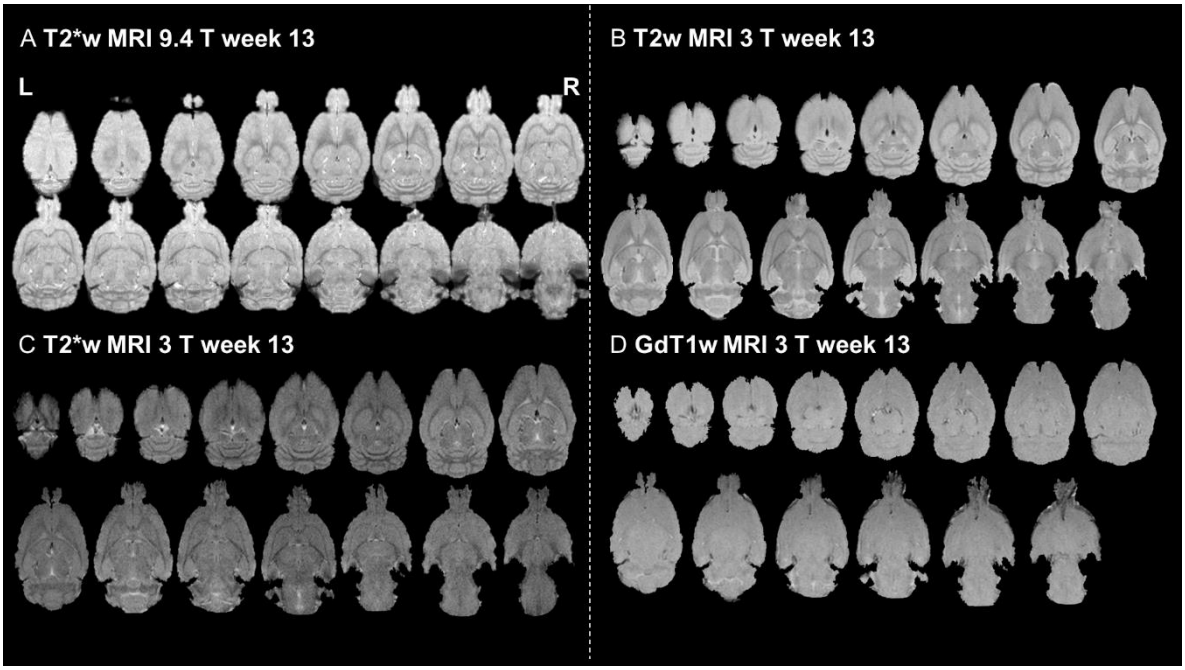

Figure S2. MRI examinations obtained at (**A)** 9.4 T or **(B-D)** 3 T for the Group B rat displayed in **Figure 2B**. (A) and (C) T2*w images at 9.4 T and 3 T from rostral to caudal sections performed at week 13 following a single course of pFUS+MB treatment appear normal. (B) T2w images at 3 T from rostral to caudal sections performed at week 13 following a single pFUS+MB treatment appear normal without abnormalities. (D) Post GdT1w images show no evidence of BBB opening. L=left, R=right.

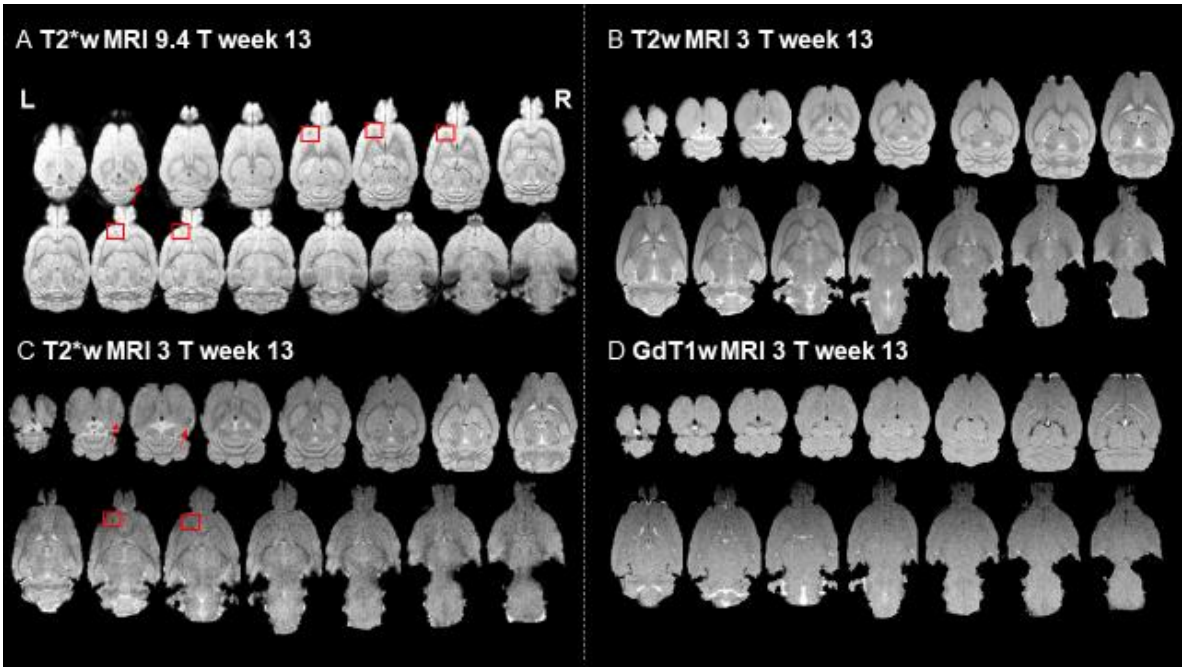

Figure S3. MRI examinations obtained at **(A)** 9.4 T or **(B-D)** 3 T for the Group B rat displayed in **Figure 2C**. (A) T2*w images from rostral to caudal sections performed at week 13 following a single course of pFUS+MB treatment showing hypointense voxels in the anterior left cortex (box) and the right hippocampus (arrow). (B) T2w images at 3 T from rostral to caudal sections performed at week 13 following a single pFUS+MB treatment appear normal without abnormalities. (C) T2*w images displays the presence of hypointense voxels in the left cortex (box) and the right hippocampus (arrow). (D) Post GdT1w images show no evidence of BBB opening. L=left, R=right.

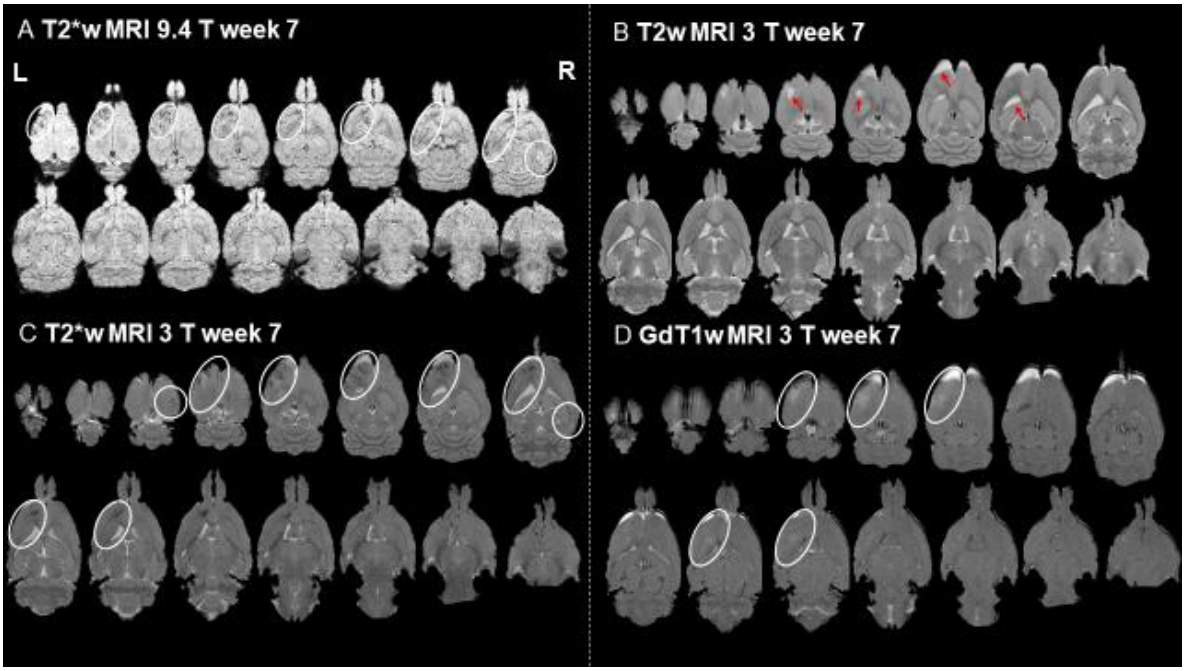

Figure S4. MRI examinations obtained at **(A)** 9.4 T or **(B-D)** 3 T for the Group C rat displayed in **Figure 3**. (A) T2*w images from rostral to caudal sections obtained at week 7 following the 6th pFUS+MB treatment showing hypointense voxels (ellipse) in the left cortex and the right hippocampus compared to the contralateral brain. Areas of hypointense voxels appear greater on the most rostral images (close to the surface of brain). (B) T2w images at 3 T from rostral to caudal sections performed at week 7 following the 6^{th} pFUS+MB treatment. MRI of the left cortex displays thickened meninges (arrow), unilateral ventriculomegaly (arrow) and hyperintense area of astrogliosis (arrow). (C) T2*w images display the presence of hypointense voxels (ellipse) in the left cortex and the right hippocampus. (D) Post GdT1w images performed 1 week after last sonication demonstrating persistent BBB disruption (ellipse) in the left cortex starting rostrally in the area of astrogliosis. L=left, R=right.

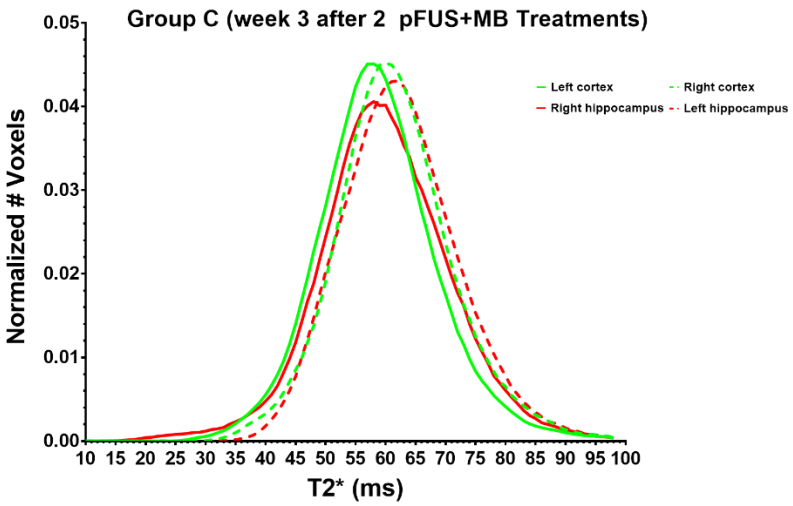

Figure S5. Calculated T2* (ms) histograms derived from T2* maps of all voxels in the sonicated and contralateral brain from Group C rats (n=6/group) after 2 pFUS+MB treatments obtained from week 3 3 T MRI scans. There was a significant difference in mean T2* values when comparing pFUS+MB treated left cortex (green line) to contralateral cortex (dashed green line) (p=0.012) and no significant differences were detected between right and left hippocampus (red line and dashed red line). See **Table S1** for descriptive statistics of histograms.

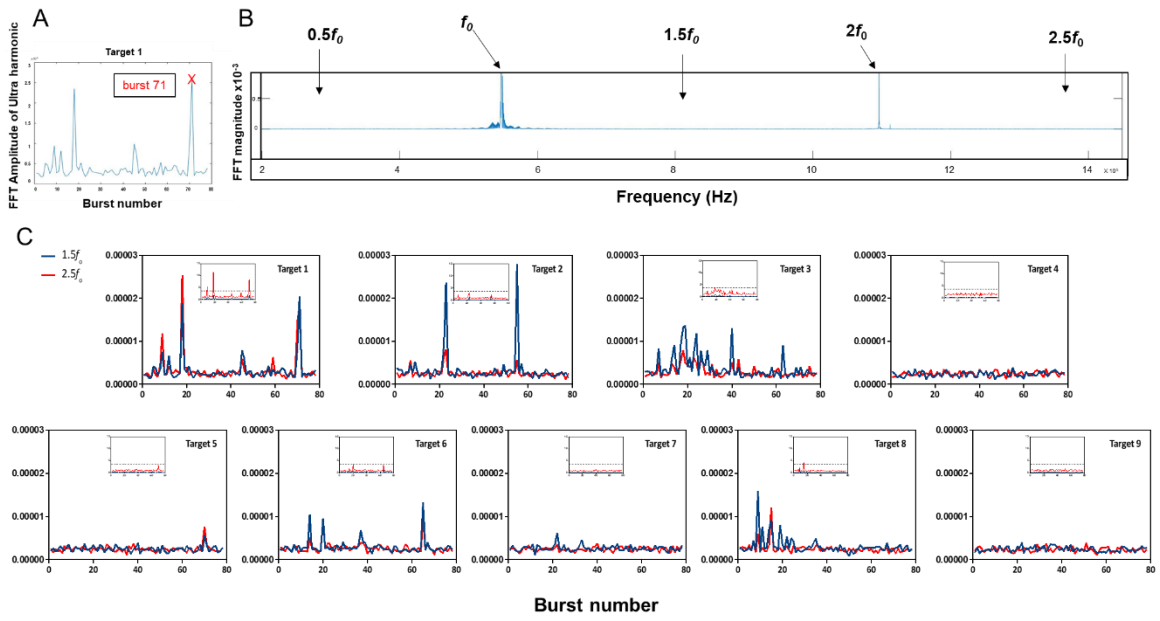

Figure S6. The center of the FUS transducer was fitted with a hydrophone (822 kHz) for passive cavitation detection (PCD) from each focal point in the left cortex and the right hippocampus. Representative PCD data was collected and processed using proprietary software from the manufacturer (FUS Instruments, Toronto, ON) and MATLAB (Mathworks, Inc, Natick, MA). **(A)** Fast Fourier Transform (FFT) magnitude spectra of 1.5*f0* ultraharmonic of all the bursts in the first target point in the cortex at PNP=0.3 MPa. **(B)** FFT magnitude spectra at all frequencies of burst 71 represents *f*0, 1.5*f0*, 2*f0* and 2.5*f0*. **(C)** FFT magnitude of the entire set of 9 target points at 1.5*f0* (blue) and 2.5*f0* (red) ultraharmonics with the insert of 1.5*f0* (blue) and 2.5*f0* (red) ratio values. The ratio values were calculated using a baseline for every target point that is the mean FFT from the first burst of every point at 1.5*f0* and 2.5*f0*. The ratio was defined as the mean FFT at each burst divided by the base mean FFT. Dashed line indicates 3.5x of the baseline FFT magnitude. FFT ratio values at 1.5*f0* and 2.5*f0* exceeding the dashed line would be consistent with excessive cavitation.

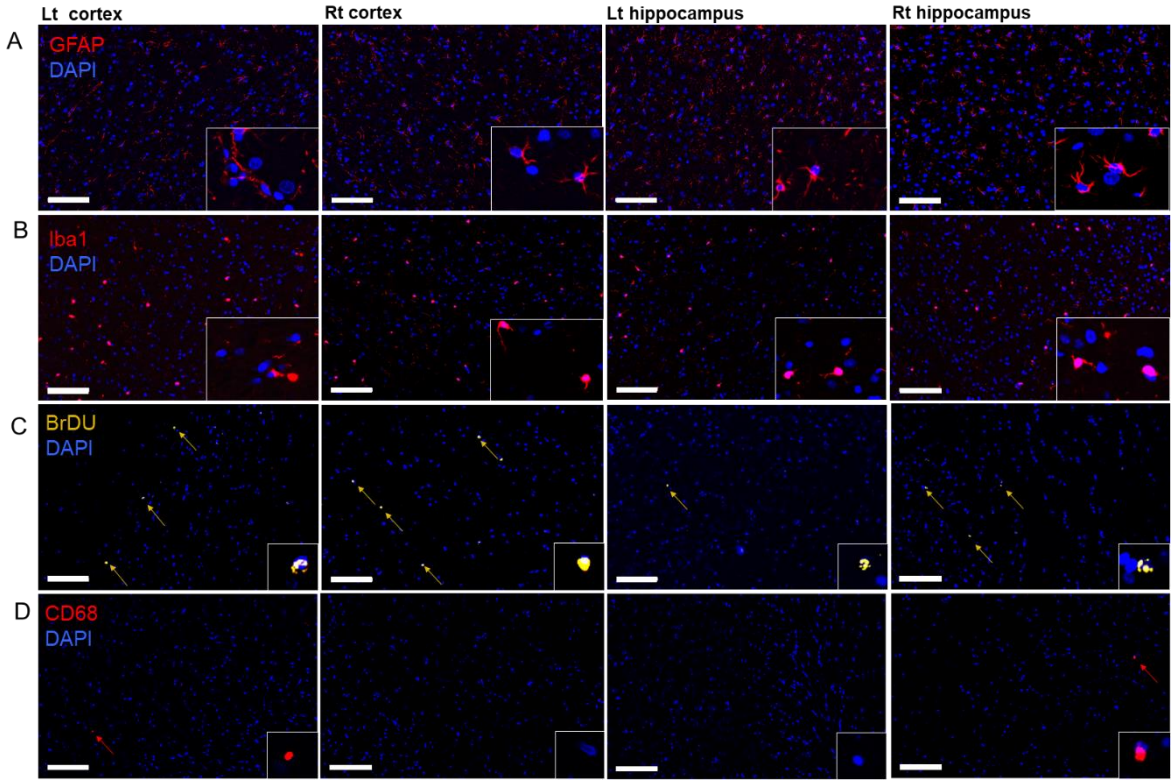

Figure S7. (A-D) Histological evaluation of a Group B rat brain 13 weeks after a single pFUS+MB treatment. (A) GFAP staining revealed little difference, whereas (B) Iba1 staining revealed essentially no difference between pFUS+MB treated versus contralateral brain. (C) Elevated numbers of $BrdU^{+}$ cells in the treated hippocampus were detected consistent with increased neurogenesis. (D) $CD68^{+}$ staining in the Lt cortex and Rt hippocampus would be consistent with the activation of innate immune response and infiltration of systemic macrophages. Scale bar=100 μm, insert is 63x magnified view of stained cells. DAPI is blue stain.

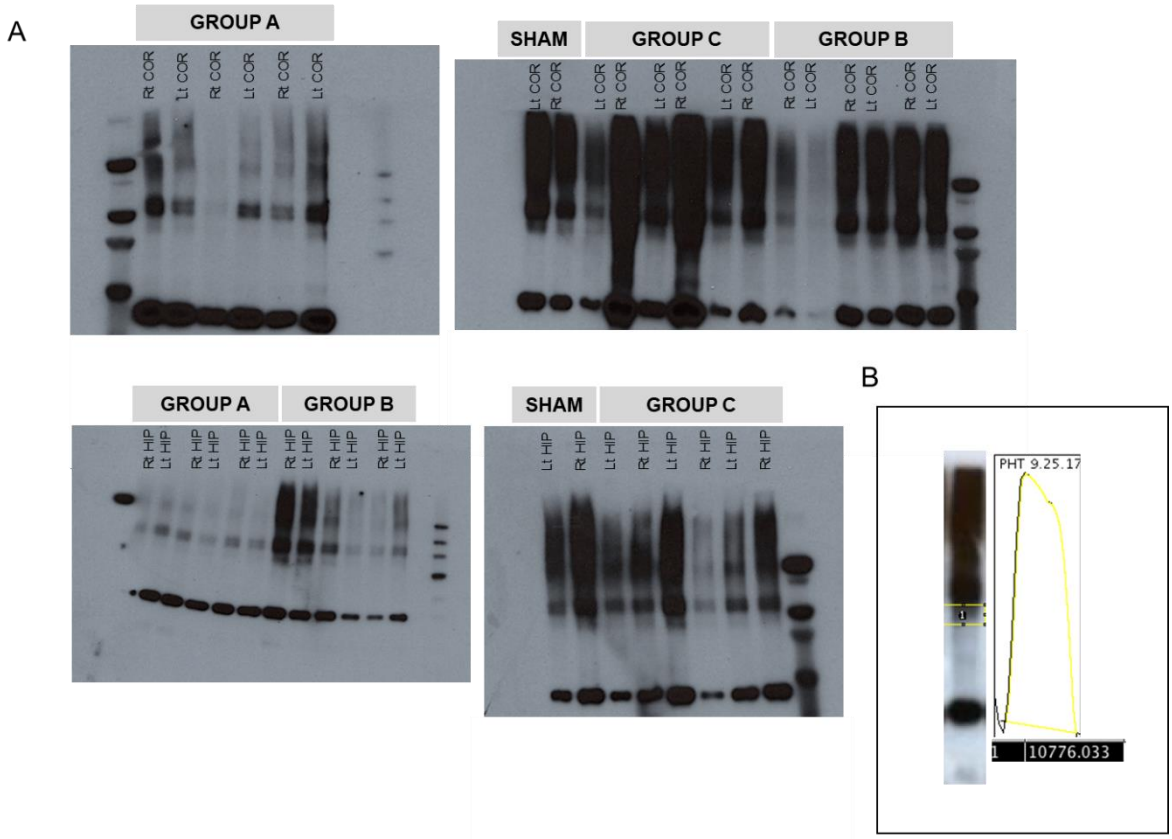

Figure S8. (A) Representative WB of sonicated (Lt COR, Rt HIP) and unsonicated (Rt COR, Lt HIP) Group A, B, C and sham brain samples. Western blots of protein originating from paraffin embedded tissue were performed in triplicates. **(B)** Densitometry analysis of the WB using Image J software, in which signal intensity of each pTau band (molecular weight: 75-100 kiliodaltons) was normalized to BA signal intensity, revealed significantly higher pTau/BA ratio in the sonicated brain of Group C animals compared to contralateral hemisphere (**Figure 8G**). The enclosed peaks in each profile plots correspond to the dark bands in the original blot.

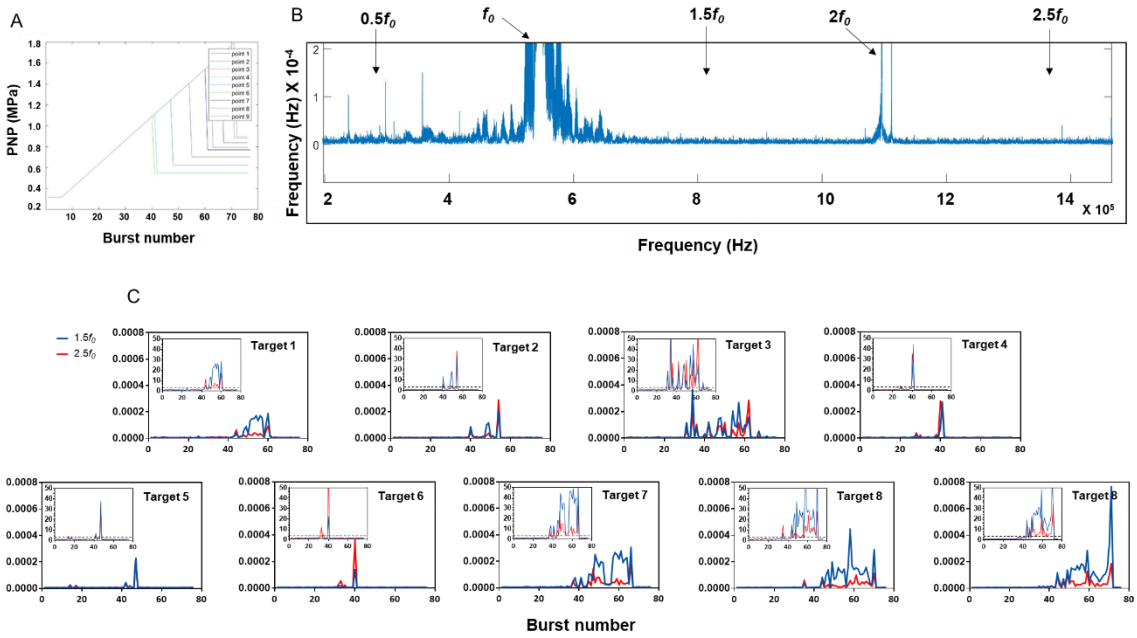

Figure S9. Representative PCD with real-time feedback-control [76] was collected during the sonication of age-matched rats. The data was processed using proprietary software from the manufacturer (FUS Instruments, Toronto, ON) and MATLAB (Mathworks, Inc, Natick, MA). **(A)** Estimated increasing in situ pressure as a function of burst number: target pressure was set to 50% to achieve ultraharmonic emissions. The pressure drop occurres at different values at each target point. **(B)** FFT magnitude spectra at all frequencies of a representative burst represents *f*0, 1.5*f0*, 2*f0* and 2.5*f0*. **(C)** FFT magnitude of the entire set of 9 target points at 1.5*f0* (blue) and 2.5*f0* (red) ultraharmonics with the insert of 1.5*f0* (blue) and 2.5*f0* (red) ratio values. The ratio values were calculated using a baseline for every target point that is the mean FFT from the first burst of every point at 1.5*f0* and 2.5*f0*. The ratio was defined as the mean FFT at each burst divided by the base mean FFT. Dashed line indicates 3.5x of the baseline FFT magnitude. FFT ratio values at 1.5*f0* and 2.5*f0* exceeding the dashed line would be consistent with excessive cavitation.

Table S1. Statistical analysis of histograms from **Figure 3** and **Figure S5** for mean T2* values, skewness and kurtosis. Left (Lt) cortex and Right (Rt) hippocampus were treated with pFUS+Optison^{TM} infusion either once (Group A and B) or by 6 weekly exposures (Group C). Data is presented as mean+standard deviation and statistical analysis was performed with paired t-test. *p=0.012, +p=0.001, !p=0.044, @p=0.009, #p=0.02.

		T2* (ms)	Skewness	Kurtosis
Group A Week 7	Lt cortex	60.2 (1.2)	0.04 (0.05)	-1.17 (0.3)
	Rt cortex	61.1 (1.2)	0.06 (0.02)	-1.17 (0.2)
	Rt hippocampus	60.9 (1.0)	-0.002 (0.04)	-1.47 (0.07)
	Lt hippocampus	60.4 (1.4)	0.002 (0.05)	-1.54 (0.04)
Group B Week 13	Lt cortex	60.4 (1.2)	0.05 (0.06)	-1.35 (0.24)
	Rt cortex	61.6 (2.8)	0.04 (0.08)	-1.44 (0.17)
	Rt hippocampus	58.5 (2.6)	0.004 (0.1)	-1.5 (0.14)
	Lt hippocampus	59.9 (1.5)	0.06 (0.04)	-1.5 (0.73)
Group C Week 3	Lt cortex	58.7 (1.5)*	0.07 (0.07)	-1.54 (0.15)
	Rt cortex	61.4 (1.2)	0.07 (0.04)	-1.48 (0.13)
	Rt hippocampus	59.9 (4.1)	0.05 (0.13)	-1.58 (0.10)
	Lt hippocampus	62.5 (3.6)	0.08 (0.03)	-1.28 (0.75)
Group C Week 7	Lt cortex	50.3 (2.4)+	-0.07 (0.02)@	-1.33 (0.12)
	Rt cortex	60.6 (3.5)	0.03 (0.05)	-1.31 (0.24)
	Rt hippocampus	53.3 (1.8)!	-0.02 (0.07)#	-1.41 (0.14)
	Lt hippocampus	58.4 (3.2)	0.07(0.04)	-1.42 (0.15)

Table S2. Summary of reports for pFUS+MB for opening BBB in rats in which pFUS PNP and dose of MB could be calculated for a 0.25 kg rat. (C=custom MB, D=Definity®, O=Optison™ (5-8x10^8 MB/mL), S=SonoVue® (1.5-5.6x10^8 MB/mL)). For Optison™ and SonoVue® the mean number of MB/mL was calculated instead of presenting the range of #MB per mL.

FUS Freq (MHz)	PNP (MPa)	MB Type	Mean # MB/mL	Dose	Units/kg (µL/kg, MB/kg)	#MB	Reference
0.5	0.62	C		4.00E+07	MB/kg	1.00E+07	[112]
0.551	0.128	D	1.20E+10	20	uL/kg	6.00E+07	[4]
0.551	0.28	D	1.20E+10	20	uL/kg	6.00E+07	[47]
3.5	0.55	D	1.20E+10	10	uL/kg	3.00E+07	[61]
3.5	0.81	D	1.20E+10	10	uL/kg	3.00E+07	
1	1	C		2.00E+08	MB/kg	5.00E+07	[113]
0.589	0.3	O	6.50E+08	100	MB	1.63E+07	[2]
0.69	0.34	O	6.50E+08	200	uL/kg	3.25E+07	[72]
0.69	0.54	O	6.50E+08	200	uL/kg	3.25E+07	
0.69	0.68	D	1.20E+10	10	uL/kg	3.00E+07	[114]
0.69	0.72	D	1.20E+10	10	uL/kg	3.00E+07	
0.4	0.32	S	3.55E+08	200	uL/kg	1.90E+07	[115]
0.4	0.88	S	3.55E+08	200	uL/kg	1.90E+07	
1	0.75	S	3.55E+08	200	uL/kg	1.90E+07	
1	1.46	S	3.55E+08	200	uL/kg	1.90E+07	
1	0.3	D	1.20E+10	200	uL/kg	6.00E+07	[116]
0.69	0.46	O	6.50E+08	100	ul/kg	1.63E+07	[117]
0.69	0.62	O	6.50E+08	100	ul/kg	1.63E+07	
1.06	0.54	O	6.50E+08	30	uL/kg	1.95E+07	[118]
1	0.6	O	6.50E+08	3.00E+08	MB/kg	7.50E+07	[119]
1	0.15	C		2.00E+07	MB/kg	5.00E+06	[120]
1	0.75	C		2.00E+07	MB/kg	5.00E+06	
1	0.7	C	5.00E+8	2.00E+07	uL/kg	1.25E+08	[121]
0.4	0.2	S	3.55E+08	100	uL/kg	9.50E+06	[122]
0.4	0.35	S	3.55E+08	100	uL/kg	9.50E+06	
0.4	0.5	S	3.55E+08	100	uL/kg	9.50E+06	
0.4	0.8	S	3.55E+08	100	uL/kg	9.50E+06	
0.5	0.36	S	3.55E+08	100	uL/kg	9.50E+06	[123]
0.5	0.7	S	3.55E+08	100	uL/kg	9.50E+06	
0.69	0.55	D	1.20E+10	10	uL/kg	3.00E+07	[124]

0.69	0.81	D	1.20E+10	10	uL/kg	3.00E+07	
1.14	0.4	C		3.50E+08	MB/kg	8.75E+07	[70]
1.14	0.6	C		3.50E+08	MB/kg	8.75E+07	
0.4	0.4	S	3.55E+08	2.4	mL/kg	8.52E+05	[62]
0.4	0.8	S	3.55E+08	2.4	mL/kg	8.52E+05	
0.48	0.57	S	3.55E+08	10	ul/kg	9.50E+05	[125]
1.2	0.4	D	1.20E+10	20	uL/kg	6.00E+07	[126]
1.2	0.6	D	1.20E+10	20	uL/kg	6.00E+07	[127]
0.558	0.4	D	1.20E+10	20	uL/kg	6.00E+07	[128]
0.69	0.55	D	1.20E+10	0.01	mL/kg	1.2E+08	[129]
0.69	0.81	D	1.20E+10	0.01	uL/kg	1.2E+08	
0.5	0.6	S	3.55E+08	100	uL/kg	8.55E+06	[130]
0.69	0.69	D	1.20E+10	10	uL/kg	3.00E+07	[131]
0.558	0.3	D	1.20E+10	20	uL/kg	6.00E+07	[132]
1.7	1.2	D	1.20E+10	1.5	uL/kg	4.50E+06	[65]
1.7	1.2	D	1.20E+10	1.5	uL/kg	4.50E+06	
0.69	0.6	D	1.20E+10	1	uL/kg	3.00E+06	[133]
0.69	0.8	D	1.20E+10	1	uL/kg	3.00E+06	
0.551	0.28	D	1.20E+10	20	uL/kg	2.4E+08	[42]
1	1.27	O	6.50E+08	100	uL/kg	1.63E+07	[134]
0.4	0.45	S	3.55E+08	2.5	uL/kg	2.38E+06	
0.4	1.35	S	3.55E+08	3.5	uL/kg	3.33E+06	[19]
1.5	0.55	S	3.55E+08	0.025	uL/kg	8.88E+06	[135]
1.5	0.78	S	3.55E+08	0.025	uL/kg	8.88E+06	
1.5	1.1	S	3.55E+08	0.025	uL/kg	8.88E+06	
1.5	1.9	S	3.55E+08	0.025	uL/kg	8.88E+06	
1.5	2.45	S	3.55E+08	0.025	uL/kg	8.88E+06	
1.5	3.47	S	3.55E+08	0.025	uL/kg	8.88E+06	
1.5	4.9	S	3.55E+08	0.025	uL/kg	8.88E+06	

References

1. Banks WA. From blood-brain barrier to blood-brain interface: new opportunities for CNS drug delivery. Nat Rev Drug Discov. 2016; 15: 275-92.
2. Kovacs ZI, Kim S, Jikaria N, Qureshi F, Milo B, Lewis BK, et al. Disrupting the blood-brain barrier by focused ultrasound induces sterile inflammation. Proc Natl Acad Sci U S A. 2017; 114: E75-E84.
3. McConnell HL, Kersch CN, Woltjer RL, Neuwelt EA. The translational significance of the neurovascular unit. J Biol Chem. 2017; 292: 762-70.
4. McMahon D, Bendayan R, Hynynen K. Acute effects of focused ultrasound-induced increases in blood-brain barrier permeability on rat microvascular transcriptome. Sci Rep. 2017; 7: 45657.
5. McMahon D, Hynynen K. Acute inflammatory response following increased blood-brain barrier permeability induced by focused ultrasound is dependent on microbubble dose. Theranostics. 2017; 7: 3989-4000.
6. Zhao Z, Nelson AR, Betsholtz C, Zlokovic BV. Establishment and dysfunction of the blood-brain barrier. Cell. 2015; 163: 1064-78.
7. Burgess A, Dubey S, Yeung S, Hough O, Eterman N, Aubert I, et al. Alzheimer disease in a mouse model: MR imaging-guided focused ultrasound targeted to the hippocampus opens the blood-brain barrier and improves pathologic abnormalities and behavior. Radiology. 2014; 273: 736-45.
8. Chapman CD, Frey WH, 2nd, Craft S, Danielyan L, Hallschmid M, Schioth HB, et al. Intranasal treatment of central nervous system dysfunction in humans. Pharm Res. 2013; 30: 2475-84.
9. Gabathuler R. Approaches to transport therapeutic drugs across the blood-brain barrier to treat brain diseases. Neurobiol Dis. 2010; 37: 48-57.
10. Gomez D, Martinez JA, Hanson LR, Frey WH, 2nd, Toth CC. Intranasal treatment of neurodegenerative diseases and stroke. Front Biosci (Schol Ed). 2012; 4: 74-89.
11. Gurlek A, Miller MJ, Amin AA, Evans GR, Reece GP, Baldwin BJ, et al. Reconstruction of complex radiation-induced injuries using free-tissue transfer. J Reconstr Microsurg. 1998; 14: 337-40.
12. Hynynen K, McDannold N, Vykhodtseva N, Jolesz FA. Noninvasive MR imaging-guided focal opening of the blood-brain barrier in rabbits. Radiology. 2001; 220: 640-6.
13. McDannold N, Vykhodtseva N, Hynynen K. Effects of acoustic parameters and ultrasound contrast agent dose on focused-ultrasound induced blood-brain barrier disruption. Ultrasound Med Biol. 2008; 34: 930-7.
14. Neuwelt E, Abbott NJ, Abrey L, Banks WA, Blakley B, Davis T, et al. Strategies to advance translational research into brain barriers. Lancet Neurol. 2008; 7: 84-96.
15. Stamatovic SM, Keep RF, Andjelkovic AV. Brain endothelial cell-cell junctions: how to "open" the blood brain barrier. Curr Neuropharmacol. 2008; 6: 179-92.
16. Suzuki Y, Nagai N, Umemura K. A Review of the mechanisms of blood-brain barrier bermeability by tissue-type plasminogen activator treatment for cerebral ischemia. Front Cell Neurosci. 2016; 10: 2.
17. Hynynen K, McDannold N, Vykhodtseva N, Jolesz FA. Non-invasive opening of BBB by focused ultrasound. Acta Neurochir Suppl. 2003; 86: 555-8.
18. Goertz DE. An overview of the influence of therapeutic ultrasound exposures on the vasculature: high intensity ultrasound and microbubble-mediated bioeffects. Int J Hyperthermia. 2015; 31: 134-44.
19. Alonso A, Reinz E, Fatar M, Jenne J, Hennerici MG, Meairs S. Neurons but not glial cells overexpress ubiquitin in the rat brain following focused ultrasound-induced opening of the blood-brain barrier. Neuroscience. 2010; 169: 116-24.
20. Kovacs ZI, Burks SR, Frank JA. Focused ultrasound with microbubbles induces sterile inflammatory response proportional to the blood brain barrier opening: Attention to experimental conditions. Theranostics. 2018; 8: 2245-8.
21. Alecou T, Giannakou M, Damianou C. Amyloid beta plaque reduction with antibodies crossing the blood-brain barrier, which was opened in 3 sessions of focused ultrasound in a rabbit model. J Ultrasound Med. 2017; 36: 2257-70.
22. Burgess A, Aubert I, Hynynen K. Focused ultrasound: crossing barriers to treat Alzheimer's disease. Ther Deliv. 2011; 2: 281-6.
23. Leinenga G, Gotz J. Scanning ultrasound removes amyloid-beta and restores memory in an Alzheimer's disease mouse model. Sci Transl Med. 2015; 7: 278ra33.
24. Meng Y, Volpini M, Black S, Lozano AM, Hynynen K, Lipsman N. Focused ultrasound as a novel strategy for Alzheimer disease therapeutics. Ann Neurol. 2017; 81: 611-7.

25. Nisbet RM, Van der Jeugd A, Leinenga G, Evans HT, Janowicz PW, Gotz J. Combined effects of scanning ultrasound and a tau-specific single chain antibody in a tau transgenic mouse model. Brain. 2017; 140: 1220-30.
26. Raymond SB, Treat LH, Dewey JD, McDannold NJ, Hynynen K, Bacskai BJ. Ultrasound enhanced delivery of molecular imaging and therapeutic agents in Alzheimer's disease mouse models. PLoS One. 2008; 3: e2175.
27. Querfurth HW, LaFerla FM. Alzheimer's disease. N Engl J Med. 2010; 362: 329-44.
28. Akiyama H, Barger S, Barnum S, Bradt B, Bauer J, Cole GM, et al. Inflammation and Alzheimer's disease. Neurobiol Aging. 2000; 21: 383-421.
29. Hong JT. NF-kB as a mediator of brain inflammation in AD. CNS Neurol Disord Drug Targets. 2017.
30. Rothwell NJ, Luheshi GN. Interleukin 1 in the brain: biology, pathology and therapeutic target. Trends Neurosci. 2000; 23: 618-25.
31. Caselli RJ, Beach TG, Knopman DS, Graff-Radford NR. Alzheimer disease: Scientific breakthroughs and translational challenges. Mayo Clin Proc. 2017; 92: 978-94.
32. Morgan D. Immunotherapy for Alzheimer's disease. J Intern Med. 2011; 269: 54-63.
33. Ruthirakuhan M, Herrmann N, Suridjan I, Abraham EH, Farber I, Lanctot KL. Beyond immunotherapy: new approaches for disease modifying treatments for early Alzheimer's disease. Expert Opin Pharmacother. 2016; 17: 2417-29.
34. Shadfar S, Hwang CJ, Lim MS, Choi DY, Hong JT. Involvement of inflammation in Alzheimer's disease pathogenesis and therapeutic potential of anti-inflammatory agents. Arch Pharm Res. 2015; 38: 2106-19.
35. Alzheimer's A. 2016 Alzheimer's disease facts and figures. Alzheimers Dement. 2016; 12: 459-509.
36. Jordao JF, Ayala-Grosso CA, Markham K, Huang Y, Chopra R, McLaurin J, et al. Antibodies targeted to the brain with image-guided focused ultrasound reduces amyloid-beta plaque load in the TgCRND8 mouse model of Alzheimer's disease. PLoS One. 2010; 5: e10549.
37. Burgess A, Eterman N, Aubert I, Hynynen K. Two-photon microscopy for real-time monitoring of focused ultrasound-mediated drug delivery to the brain in a mouse model of Alzheimer's disease. Proc Spie. 2013; 8588.
38. Jordao JF, Thevenot E, Markham-Coultes K, Scarcelli T, Weng YQ, Xhima K, et al. Amyloid-beta plaque reduction, endogenous antibody delivery and glial activation by brain-targeted, transcranial focused ultrasound. Exp Neurol. 2013; 248: 16-29.
39. National Research Council (U.S.). Committee for the update of the guide for the care and use of laboratory animals. 8th ed. Washington, D.C.: Institute for Laboratory Animal Research (U.S.) & National Academies Press (U.S.); 2011.
40. Tu TW, Turtzo LC, Williams RA, Lescher JD, Dean DD, Frank JA. Imaging of spontaneous ventriculomegaly and vascular malformations in Wistar rats: implications for preclinical research. J Neuropathol Exp Neurol. 2014; 73: 1152-65.
41. Wojtowicz JM, Kee N. BrdU assay for neurogenesis in rodents. Nat Protoc. 2006; 1: 1399-405.
42. O'Reilly MA, Hynynen K. Blood-brain barrier: real-time feedback-controlled focused ultrasound disruption by using an acoustic emissions-based controller. Radiology. 2012; 263: 96-106.
43. Anderson SA, Glod J, Arbab AS, Noel M, Ashari P, Fine HA, et al. Noninvasive MR imaging of magnetically labeled stem cells to directly identify neovasculature in a glioma model. Blood. 2005; 105: 420-5.
44. Fix SM, Nyankima AG, McSweeney MD, Tsuruta JK, Lai SK, Dayton PA. Accelerated Clearance of Ultrasound Contrast Agents Containing Polyethylene Glycol is Associated with the Generation of Anti-Polyethylene Glycol Antibodies. Ultrasound Med Biol. 2018; 44: 1266-80.
45. Horodyckid C, Canney M, Vignot A, Boisgard R, Drier A, Huberfeld G, et al. Safe long-term repeated disruption of the blood-brain barrier using an implantable ultrasound device: a multiparametric study in a primate model. J Neurosurg. 2017; 126: 1351-61.
46. Kroll RA, Neuwelt EA. Outwitting the blood-brain barrier for therapeutic purposes: osmotic opening and other means. Neurosurgery. 1998; 42: 1083-99; discussion 99-100.
47. O'Reilly MA, Jones RM, Barrett E, Schwab A, Head E, Hynynen K. Investigation of the safety of focused ultrasound-induced blood-brain barrier opening in a natural canine model of aging. Theranostics. 2017; 7: 3573-84.
48. Kovacs Z, Werner B, Rassi A, Sass JO, Martin-Fiori E, Bernasconi M. Prolonged survival upon ultrasound-enhanced doxorubicin delivery in two syngenic glioblastoma mouse models. J Control Release. 2014; 187: 74-82.
49. Downs ME, Buch A, Karakatsani ME, Konofagou EE, Ferrera VP. Blood-brain barrier opening in behaving non-human primates via focused ultrasound with systemically administered microbubbles. Sci Rep. 2015; 5: 15076.

50. Downs ME, Buch A, Sierra C, Karakatsani ME, Teichert T, Chen S, et al. Long-term safety of repeated blood-brain barrier opening via focused ultrasound with microbubbles in non-human primates performing a cognitive task. PLoS One. 2015; 10: e0125911.
51. Olumolade OO, Wang S, Samiotaki G, Konofagou EE. Longitudinal motor and behavioral assessment of blood-brain barrier opening with transcranial focused ultrasound. Ultrasound Med Biol. 2016; 42: 2270-82.
52. Kobus T, Vykhodtseva N, Pilatou M, Zhang Y, McDannold N. Safety validation of repeated blood-brain barrier disruption using focused ultrasound. Ultrasound Med Biol. 2016; 42: 481-92.
53. Kovacs ZI, Burks SR, Frank JA. Reply to Silburt et al.: Concerning sterile inflammation following focused ultrasound and microbubbles in the brain. Proc Natl Acad Sci U S A. 2017: PMC5565475.
54. Silburt J, Lipsman N, Aubert I. Disrupting the blood-brain barrier with focused ultrasound: Perspectives on inflammation and regeneration. Proc Natl Acad Sci U S A. 2017: PMC5565470.
55. Amantea D, Micieli G, Tassorelli C, Cuartero MI, Ballesteros I, Certo M, et al. Rational modulation of the innate immune system for neuroprotection in ischemic stroke. Front Neurosci. 2015; 9: 147.
56. Chen GY, Nunez G. Sterile inflammation: sensing and reacting to damage. Nat Rev Immunol. 2010; 10: 826-37.
57. Denes A, Thornton P, Rothwell NJ, Allan SM. Inflammation and brain injury: acute cerebral ischaemia, peripheral and central inflammation. Brain Behav Immun. 2010; 24: 708-23.
58. Gadani SP, Walsh JT, Lukens JR, Kipnis J. Dealing with danger in the CNS: The response of the immune system to injury. Neuron. 2015; 87: 47-62.
59. Tuttolomondo A, Pecoraro R, Pinto A. Studies of selective TNF inhibitors in the treatment of brain injury from stroke and trauma: a review of the evidence to date. Drug Des Devel Ther. 2014; 8: 2221-38.
60. Moonen CT, van Zijl PC, Frank JA, Le Bihan D, Becker ED. Functional magnetic resonance imaging in medicine and physiology. Science. 1990; 250: 53-61.
61. Aryal M, Fischer K, Gentile C, Gitto S, Zhang YZ, McDannold N. Effects on p-glycoprotein expression after blood-brain barrier disruption using focused ultrasound and microbubbles. PLoS One. 2017; 12: e0166061.
62. Chai WY, Chu PC, Tsai MY, Lin YC, Wang JJ, Wei KC, et al. Magnetic-resonance imaging for kinetic analysis of permeability changes during focused ultrasound-induced blood-brain barrier opening and brain drug delivery. J Control Release. 2014; 192: 1-9.
63. McDannold N, Zhang Y, Vykhodtseva N. Nonthermal ablation in the rat brain using focused ultrasound and an ultrasound contrast agent: long-term effects. J Neurosurg. 2016; 125: 1539-48.
64. Treat LH, McDannold N, Vykhodtseva N, Zhang YZ, Tam K, Hynynen K. Targeted delivery of doxorubicin to the rat brain at therapeutic levels using MRI-guided focused ultrasound. Int J Cancer. 2007; 121: 901-7.
65. Treat LH, McDannold N, Zhang Y, Vykhodtseva N, Hynynen K. Improved anti-tumor effect of liposomal doxorubicin after targeted blood-brain barrier disruption by MRI-guided focused ultrasound in rat glioma. Ultrasound Med Biol. 2012; 38: 1716-25.
66. Tu TW, Ibrahim WG, Jikaria N, Munasinghe JP, Witko JA, Hammoud DA, et al. On the detection of cerebral metabolic depression in experimental traumatic brain injury using Chemical Exchange Saturation Transfer (CEST)-weighted MRI. Sci Rep. 2018; 8: 669.
67. Wang Y, Wang Q, Haldar JP, Yeh FC, Xie M, Sun P, et al. Quantification of increased cellularity during inflammatory demyelination. Brain. 2011; 134: 3590-601.
68. Sun P, Murphy RK, Gamble P, George A, Song SK, Ray WZ. Diffusion assessment of cortical changes, induced by traumatic spinal cord injury. Brain Sci. 2017; 7.
69. Tu TW, Williams RA, Lescher JD, Jikaria N, Turtzo LC, Frank JA. Radiological-pathological correlation of diffusion tensor and magnetization transfer imaging in a closed head traumatic brain injury model. Ann Neurol. 2016; 79: 907-20.
70. Nance E, Timbie K, Miller GW, Song J, Louttit C, Klibanov AL, et al. Non-invasive delivery of stealth, brain-penetrating nanoparticles across the blood-brain barrier using MRI-guided focused ultrasound. J Control Release. 2014; 189: 123-32.
71. Itani M, Mattrey RF. The effect of inhaled gases on ultrasound contrast agent longevity in vivo. Mol Imaging Biol. 2012; 14: 40-6.
72. McDannold N, Zhang Y, Vykhodtseva N. The effects of oxygen on ultrasound-induced blood-brain barrier disruption in mice. Ultrasound Med Biol. 2017; 43: 469-75.
73. Mullin L, Gessner R, Kwan J, Kaya M, Borden MA, Dayton PA. Effect of anesthesia carrier gas on in vivo circulation times of ultrasound microbubble contrast agents in rats. Contrast Media Mol Imaging. 2011; 6: 126-31.
74. McMahon D, Hynynen K. Reply to Kovacs et al.: Concerning acute inflammatory response following focused ultrasound and microbubbles in the brain Theranostics. 2018; 8: 2249-50.

75. Sun T, Zhang Y, Power C, Alexander PM, Sutton JT, Aryal M, et al. Closed-loop control of targeted ultrasound drug delivery across the blood-brain/tumor barriers in a rat glioma model. Proc Natl Acad Sci U S A. 2017; 114: E10281-E90.
76. O'Reilly MA, Hough O, Hynynen K. Blood-brain barrier closure time after controlled ultrasound-induced opening is independent of opening volume. J Ultrasound Med. 2017; 36: 475-83.
77. Sierra C, Acosta C, Chen C, Wu SY, Karakatsani ME, Bernal M, et al. Lipid microbubbles as a vehicle for targeted drug delivery using focused ultrasound-induced blood-brain barrier opening. J Cereb Blood Flow Metab. 2017; 37: 1236-50.
78. Fuger P, Hefendehl JK, Veeraraghavalu K, Wendeln AC, Schlosser C, Obermuller U, et al. Microglia turnover with aging and in an Alzheimer's model via long-term in vivo single-cell imaging. Nat Neurosci. 2017; 20: 1371-6.
79. Hefendehl JK, Neher JJ, Suhs RB, Kohsaka S, Skodras A, Jucker M. Homeostatic and injury-induced microglia behavior in the aging brain. Aging Cell. 2014; 13: 60-9.
80. Yulug B, Hanoglu L, Kilic E. The neuroprotective effect of focused ultrasound: New perspectives on an old tool. Brain Res Bull. 2017; 131: 199-206.
81. Cao L, Jiao X, Zuzga DS, Liu Y, Fong DM, Young D, et al. VEGF links hippocampal activity with neurogenesis, learning and memory. Nat Genet. 2004; 36: 827-35.
82. Leinenga G, Langton C, Nisbet R, Gotz J. Ultrasound treatment of neurological diseases--current and emerging applications. Nat Rev Neurol. 2016; 12: 161-74.
83. Marti HH. Erythropoietin and the hypoxic brain. J Exp Biol. 2004; 207: 3233-42.
84. Reher P, Doan N, Bradnock B, Meghji S, Harris M. Effect of ultrasound on the production of IL-8, basic FGF and VEGF. Cytokine. 1999; 11: 416-23.
85. Scarcelli T, Jordao JF, O'Reilly MA, Ellens N, Hynynen K, Aubert I. Stimulation of hippocampal neurogenesis by transcranial focused ultrasound and microbubbles in adult mice. Brain Stimul. 2014; 7: 304-7.
86. Stumm RK, Rummel J, Junker V, Culmsee C, Pfeiffer M, Krieglstein J, et al. A dual role for the SDF-1/CXCR4 chemokine receptor system in adult brain: isoform-selective regulation of SDF-1 expression modulates CXCR4-dependent neuronal plasticity and cerebral leukocyte recruitment after focal ischemia. J Neurosci. 2002; 22: 5865-78.
87. Tufail Y, Matyushov A, Baldwin N, Tauchmann ML, Georges J, Yoshihiro A, et al. Transcranial pulsed ultrasound stimulates intact brain circuits. Neuron. 2010; 66: 681-94.
88. Iqbal K, Liu F, Gong CX. Tau and neurodegenerative disease: the story so far. Nat Rev Neurol. 2016; 12: 15-27.
89. Mez J, Daneshvar DH, Kiernan PT, Abdolmohammadi B, Alvarez VE, Huber BR, et al. Clinicopathological evaluation of chronic traumatic encephalopathy in players of american football. JAMA. 2017; 318: 360-70.
90. Noble W, Hanger DP, Miller CC, Lovestone S. The importance of tau phosphorylation for neurodegenerative diseases. Front Neurol. 2013; 4: 83.
91. Turner RC, Lucke-Wold BP, Logsdon AF, Robson MJ, Dashnaw ML, Huang JH, et al. The quest to model chronic traumatic encephalopathy: A multiple model and injury paradigm experience. Front Neurol. 2015; 6: 222.
92. Wang Y, Mandelkow E. Tau in physiology and pathology. Nat Rev Neurosci. 2016; 17: 5-21.
93. Hernandez F, Lucas JJ, Avila J. GSK3 and tau: two convergence points in Alzheimer's disease. J Alzheimers Dis. 2013; 33 Suppl 1: S141-4.
94. Kohler C, Dinekov M, Gotz J. Active glycogen synthase kinase-3 and tau pathology-related tyrosine phosphorylation in pR5 human tau transgenic mice. Neurobiol Aging. 2013; 34: 1369-79.
95. Baseri B, Choi JJ, Deffieux T, Samiotaki G, Tung YS, Olumolade O, et al. Activation of signaling pathways following localized delivery of systemically administered neurotrophic factors across the blood-brain barrier using focused ultrasound and microbubbles. Phys Med Biol. 2012; 57: N65-81.
96. Jalali S, Huang Y, Dumont DJ, Hynynen K. Focused ultrasound-mediated bbb disruption is associated with an increase in activation of AKT: experimental study in rats. BMC Neurol. 2010; 10: 114.
97. Bellucci A, Bugiani O, Ghetti B, Spillantini MG. Presence of reactive microglia and neuroinflammatory mediators in a case of frontotemporal dementia with P301S mutation. Neurodegener Dis. 2011; 8: 221-9.
98. Hawkins BE, Krishnamurthy S, Castillo-Carranza DL, Sengupta U, Prough DS, Jackson GR, et al. Rapid accumulation of endogenous tau oligomers in a rat model of traumatic brain injury: possible link between traumatic brain injury and sporadic tauopathies. J Biol Chem. 2013; 288: 17042-50.
99. McAteer KM, Corrigan F, Thornton E, Turner RJ, Vink R. Short and long term behavioral and pathological changes in a novel rodent model of repetitive mild traumatic brain injury. PLoS One. 2016; 11: e0160220.

100. McKee AC, Cantu RC, Nowinski CJ, Hedley-Whyte ET, Gavett BE, Budson AE, et al. Chronic traumatic encephalopathy in athletes: progressive tauopathy after repetitive head injury. J Neuropathol Exp Neurol. 2009; 68: 709-35.
101. Roth TL, Nayak D, Atanasijevic T, Koretsky AP, Latour LL, McGavern DB. Transcranial amelioration of inflammation and cell death after brain injury. Nature. 2014; 505: 223-8.
102. Russo MV, McGavern DB. Immune Surveillance of the CNS following infection and injury. Trends Immunol. 2015; 36: 637-50.
103. Louveau A, Smirnov I, Keyes TJ, Eccles JD, Rouhani SJ, Peske JD, et al. Structural and functional features of central nervous system lymphatic vessels. Nature. 2015; 523: 337-41.
104. Head E, Murphey HL, Dowling AL, McCarty KL, Bethel SR, Nitz JA, et al. A combination cocktail improves spatial attention in a canine model of human aging and Alzheimer's disease. J Alzheimers Dis. 2012; 32: 1029-42.
105. Smith DH, Chen XH, Nonaka M, Trojanowski JQ, Lee VM, Saatman KE, et al. Accumulation of amyloid beta and tau and the formation of neurofilament inclusions following diffuse brain injury in the pig. J Neuropathol Exp Neurol. 1999; 58: 982-92.
106. Fung LK. A sterile animal model for neuroinflammation? Sci Transl Med. 2017; 9: eaa14994.
107. O'Reilly MA, Huang Y, Hynynen K. The impact of standing wave effects on transcranial focused ultrasound disruption of the blood-brain barrier in a rat model. Phys Med Biol. 2010; 55: 5251-67.
108. Aryal M, Vykhodtseva N, Zhang YZ, McDannold N. Multiple sessions of liposomal doxorubicin delivery via focused ultrasound mediated blood-brain barrier disruption: a safety study. J Control Release. 2015; 204: 60-9.
109. McDannold N, Arvanitis CD, Vykhodtseva N, Livingstone MS. Temporary disruption of the blood-brain barrier by use of ultrasound and microbubbles: safety and efficacy evaluation in rhesus macaques. Cancer Res. 2012; 72: 3652-63.
110. Samiotaki G, Konofagou EE. Dependence of the reversibility of focused- ultrasound-induced blood-brain barrier opening on pressure and pulse length in vivo. IEEE Trans Ultrason Ferroelectr Freq Control. 2013; 60: 2257-65.
111. Lee DE, Yue X, Ibrahim WG, Lentz MR, Peterson KL, Jagoda EM, et al. Lack of neuroinflammation in the HIV-1 transgenic rat: an [(18)F]-DPA714 PET imaging study. J Neuroinflammation. 2015; 12: 171.
112. Wu SK, Chu PC, Chai WY, Kang ST, Tsai CH, Fan CH, et al. Characterization of different microbubbles in assisting focused ultrasound-induced blood-brain barrier opening. Sci Rep. 2017; 7: 46689.
113. Song KH, Fan AC, Hinkle JJ, Newman J, Borden MA, Harvey BK. Microbubble gas volume: A unifying dose parameter in blood-brain barrier opening by focused ultrasound. Theranostics. 2017; 7: 144-52.
114. Park J, Aryal M, Vykhodtseva N, Zhang YZ, McDannold N. Evaluation of permeability, doxorubicin delivery, and drug retention in a rat brain tumor model after ultrasound-induced blood-tumor barrier disruption. J Control Release. 2017; 250: 77-85.
115. Chu PC, Chai WY, Tsai CH, Kang ST, Yeh CK, Liu HL. Focused ultrasound-induced blood-brain barrier opening: Association with mechanical index and cavitation index analyzed by dynamic contrast-enhanced magnetic-resonance imaging. Sci Rep. 2016; 6: 33264.
116. Cho H, Lee HY, Han M, Choi JR, Ahn S, Lee T, et al. Localized down-regulation of p-glycoprotein by focused ultrasound and microbubbles induced blood-brain barrier disruption in rat brain. Sci Rep. 2016; 6: 31201.
117. Kobus T, Zervantonakis IK, Zhang Y, McDannold NJ. Growth inhibition in a brain metastasis model by antibody delivery using focused ultrasound-mediated blood-brain barrier disruption. J Control Release. 2016; 238: 281-8.
118. Mulik RS, Bing C, Ladouceur-Wodzak M, Munaweera I, Chopra R, Corbin IR. Localized delivery of low-density lipoprotein docosahexaenoic acid nanoparticles to the rat brain using focused ultrasound. Biomaterials. 2016; 83: 257-68.
119. Mead BP, Mastorakos P, Suk JS, Klibanov AL, Hanes J, Price RJ. Targeted gene transfer to the brain via the delivery of brain-penetrating DNA nanoparticles with focused ultrasound. J Control Release. 2016; 223: 109-17.
120. Aslund AKO, Berg S, Hak S, Morch Y, Torp SH, Sandvig A, et al. Nanoparticle delivery to the brain--By focused ultrasound and self-assembled nanoparticle-stabilized microbubbles. J Control Release. 2015; 220: 287-94.
121. Su WS, Tsai ML, Huang SL, Liu SH, Yang FY. Controllable permeability of blood-brain barrier and reduced brain injury through low-intensity pulsed ultrasound stimulation. Oncotarget. 2015; 6: 42290-9.
122. Chu PC, Liu HL, Lai HY, Lin CY, Tsai HC, Pei YC. Neuromodulation accompanying focused ultrasound-induced blood-brain barrier opening. Sci Rep. 2015; 5: 15477.

123. Chen PY, Hsieh HY, Huang CY, Lin CY, Wei KC, Liu HL. Focused ultrasound-induced blood-brain barrier opening to enhance interleukin-12 delivery for brain tumor immunotherapy: a preclinical feasibility study. J Transl Med. 2015; 13: 93.
124. Aryal M, Park J, Vykhodtseva N, Zhang YZ, McDannold N. Enhancement in blood-tumor barrier permeability and delivery of liposomal doxorubicin using focused ultrasound and microbubbles: evaluation during tumor progression in a rat glioma model. Phys Med Biol. 2015; 60: 2511-27.
125. Wu SK, Yang MT, Kang KH, Liou HC, Lu DH, Fu WM, et al. Targeted delivery of erythropoietin by transcranial focused ultrasound for neuroprotection against ischemia/reperfusion-induced neuronal injury: a long-term and short-term study. PLoS One. 2014; 9: e90107.
126. Nhan T, Burgess A, Cho EE, Stefanovic B, Lilge L, Hynynen K. Drug delivery to the brain by focused ultrasound induced blood-brain barrier disruption: quantitative evaluation of enhanced permeability of cerebral vasculature using two-photon microscopy. J Control Release. 2013; 172: 274-80.
127. Alkins RD, Brodersen PM, Sodhi RN, Hynynen K. Enhancing drug delivery for boron neutron capture therapy of brain tumors with focused ultrasound. Neuro-oncology. 2013; 15: 1225-35.
128. Chu PC, Chai WY, Hsieh HY, Wang JJ, Wey SP, Huang CY, et al. Pharmacodynamic analysis of magnetic resonance imaging-monitored focused ultrasound-induced blood-brain barrier opening for drug delivery to brain tumors. BioMed Res Int. 2013; 2013: 627496.
129. Aryal M, Vykhodtseva N, Zhang YZ, Park J, McDannold N. Multiple treatments with liposomal doxorubicin and ultrasound-induced disruption of blood-tumor and blood-brain barriers improve outcomes in a rat glioma model. J Control Release. 2013; 169: 103-11.
130. Wei KC, Chu PC, Wang HY, Huang CY, Chen PY, Tsai HC, et al. Focused ultrasound-induced blood-brain barrier opening to enhance temozolomide delivery for glioblastoma treatment: a preclinical study. PLoS One. 2013; 8: e58995.
131. Park EJ, Zhang YZ, Vykhodtseva N, McDannold N. Ultrasound-mediated blood-brain/blood-tumor barrier disruption improves outcomes with trastuzumab in a breast cancer brain metastasis model. J Control Release. 2012; 163: 277-84.
132. Burgess A, Huang Y, Querbes W, Sah DW, Hynynen K. Focused ultrasound for targeted delivery of siRNA and efficient knockdown of Htt expression. J Control Release. 2012; 163: 125-9.
133. Park J, Zhang Y, Vykhodtseva N, Jolesz FA, McDannold NJ. The kinetics of blood brain barrier permeability and targeted doxorubicin delivery into brain induced by focused ultrasound. J Control Release. 2012; 162: 134-42.
134. Liu HL, Hua MY, Chen PY, Chu PC, Pan CH, Yang HW, et al. Blood-brain barrier disruption with focused ultrasound enhances delivery of chemotherapeutic drugs for glioblastoma treatment. Radiology. 2010; 255: 415-25.
135. Liu HL, Wai YY, Chen WS, Chen JC, Hsu PH, Wu XY, et al. Hemorrhage detection during focused-ultrasound induced blood-brain-barrier opening by using susceptibility-weighted magnetic resonance imaging. Ultrasound Med Biol. 2008; 34: 598-606.